JBC ARTICLE

The exercise cytokine interleukin-15 rescues slow wound healing in aged mice

Received for publication, August 20, 2019, and in revised form, November 12, 2019 Published, Papers in Press, November 20, 2019, DOI 10.1074/jbc.RA119.010740

Wesley Wong, Elizabeth D. Crane, Yikai Kuo, Austin Kim, and Justin D. Crane[1]

From the Department of Biology, Northeastern University, Boston, Massachusetts 02115

Edited by Luke O'Neill

Impaired wound healing in elderly individuals increases infection risk and prolongs surgical recovery, but current treatment options are limited. Low doses of interleukin-15 (IL-15) that mimic exercise responses in the circulation improve skin structure and increase mitochondria in uninjured aged skin, suggesting that IL-15 is an essential mitochondrial signal for healing that is lost during aging. Here we used gene microarray analysis of old and young murine epidermal stem cells and demonstrate that aging results in a gene signature characteristic of bioenergetic dysfunction. Intravenous IL-15 treatment rescued chronological aging-induced healing defects and restored youthful wound closure in old, sedentary mice. Additionally, exercise-mediated improvements in the healing of aged skin depend upon circulating IL-15. We show that IL-15 induces signal transducer and activator of transcription 3 (STAT3) signaling characteristic of young animals, reduces markers of growth arrest, and increases keratinocyte and fibroblast growth. Moreover, exercise or exercise-mimicking IL-15 treatment rescued the age-associated decrease in epidermal mitochondrial complex IV activity. Overall, these results indicate that IL-15 or its analogs represent promising therapies for treating impaired wound healing in elderly patients.

The integrity of the skin barrier is critical for blocking pathogens and other environmental hazards and the proper maintenance of skin structure requires timely, coordinated tissue repair. Skin healing is complex and requires the coordination of clotting, the recruitment of multiple types of immune cells, and significant amounts of tissue re-growth (1). Skin trauma is repaired relatively quickly in young skin, however, in the elderly wounds heal more slowly (2) and this older population is particularly susceptible to nonhealing, chronic wounds (3, 4). Delays in skin healing dramatically increase the risk of infection, prolong recovery from surgery, and increase morbidity and mortality in older adults (5). As a result, the care and management of nonhealing ulcers or poorly healing wounds costs approximately $10–25 billion per year in the United States alone (6). Overall, improving skin healing in the elderly is a major challenge for medicine and new treatment strategies are needed.

Aging is broadly associated with various forms of cellular dysfunction such as genomic instability, inflammation, and stem cell dysfunction (7, 8). Although the mechanisms responsible for poor healing remain unclear, there is evidence that aging delays epidermal stem cell activation (9, 10), shifts immune cell populations (11), and alters vascular repair after injury (12). In association with these changes aged skin exhibits epidermal and dermal thinning, has lower rates of post-injury keratinocyte proliferation, and experiences slowed wound re-epithelialization. Past work has employed expression profiling of aged keratinocytes to better understand the mechanisms of epidermal dysfunction and these data suggest that changes in the cell cycle, disrupted cytokine signaling, and altered growth cues may prevent rapid healing (9). As a result of this work, keratinocyte signal transducer and activator of transcription 3 (STAT3)[2] was identified as a promising target for reversing age-induced healing defects as it is required for re-epithelialization after skin injury (13) and dysfunctional STAT3 signaling at the wound edge is thought to impede keratinocyte proliferation in old mice (9). However, we do not understand what triggers age-related changes in keratinocyte STAT3 signaling over the lifespan and we currently lack treatments that can restore this pathway and augment healing in aged skin.

Several therapeutic approaches have been identified that improve skin healing and reduce scarring in young, healthy skin, such as negative pressure therapy, cellular scaffolds or supplemental growth factors, however, none of these therapies has proven effective at reversing healing defects in aged skin (14). There are several roadblocks to developing effective healing treatments for the elderly: 1) few studies specifically target intrinsic, aging-induced cellular dysfunction; 2) aged skin cells have impaired signal transduction responses (15), which may reduce the effectiveness of growth factors or other mitogenic treatments in aged skin; 3) excessive exposure to exogenous growth factors may cause the malignant transformation of cells or promote tumor growth in aged, cancer-prone cells. Thus, it

This work was supported by startup funding from the Northeastern University Provost's Office (to J. D. C.). J. D. C. is a co-holder of a patent involving the use of IL-15 as a therapy for skin disorders.

This article contains Figs. S1–S4.

[1] To whom correspondence should be addressed: Dept. of Biology, 360 Huntington Ave., Northeastern University, Boston, MA 02115. Tel.: 617-373-6581; E-mail: j.crane@northeastern.edu.

[2] The abbreviations used are: STAT3, signal transducer and activator of transcription 3; ESC, epidermal stem cell; GAGE, generally applicable gene set enrichment for pathway analysis; GSEA, gene set enrichment analysis; EdU, 5-ethynyl-2′-deoxyuridine; HMG, high mobility group; mtDNA, mitochondrial DNA; PolG mice, polymerase γ mutator mice; TBS, Tris-buffered saline; IL- interleukin; rmIL-15, recombinant mouse IL-15; BrdU, bromodeoxyuridine; Tricine, *N*-[2-hydroxy-1,1-bis(hydroxymethyl)ethyl]glycine; DAPI, 4′,6-diamidino-2-phenylindole; qPCR, quantitative PCR ; AMPK, AMP-activated protein kinase; PPAR, peroxisome proliferator-activated receptor.

may be more prudent to first focus on treating the pathophysiology of skin aging to curtail healing defects. In a similar vein, we reasoned that therapies known to successfully reverse skin aging would also improve poor skin healing.

Aerobic exercise is a robust lifestyle intervention that produces widespread health benefits over the lifespan including reduced mortality and a lower incidence of neurologic, cardiovascular, and cancer-related disease (16). Notably, pre- and post-operative exercise is associated with improved recovery from various types of surgery in elderly adults (17). Exercise is also one of the few interventions shown to enhance wound healing in the aged skin of both mice (18) and humans (19), however, the mechanism underlying these benefits is not known. Because exercise has such a well-established safety profile to protect against systemic disease, mimicking exercise signaling is an ideal way to treat age-related disorders, particularly in the frail elderly that are unable to exercise. We previously discovered that regular exercise reverses some of the structural effects of epidermal and dermal aging in the skin and increases the abundance of skin mitochondria in humans and mice (20). By screening the blood of athletes, we identified exercise-induced IL-15 as the circulating signal that increases skin mitochondria. Additionally, we found that a low, exercise-mimicking dose of recombinant mouse IL-15 (rmIL-15; 25 ng/kg) provided daily for 5 weeks to old mice was sufficient to improve skin structure, restore tissue mitochondrial abundance, and reduce circulating inflammatory cytokines akin to exercise (20). This was of interest because IL-15 is considered pro-inflammatory and induces T-cell proliferation (21). Conversely, regular exercise is broadly anti-inflammatory (22), but stimulates far lower levels of IL-15 in circulation than the concentrations associated with innate immune responses (20). Overall, these data suggested that increasing mitochondrial abundance in the skin is a potential way to treat skin aging and that the low pulses of IL-15 stimulated by exercise are a physiologic regulator of skin mitochondria. As circulating levels of IL-15 are reduced in aged mice (23) and disrupted IL-15 signaling is observed in nonhealing human wounds (24), we reasoned that our low-dose rmIL-15 therapy may restore youthful signaling and improve healing in aged animals.

We show that daily, low-dose injections of rmIL-15 restore youthful wound closure, increase mitochondrial activity, reduce cellular senescence, and normalize STAT3 signaling in aged, sedentary mice. Additionally, we find that the improvement in wound re-epithelialization observed in old, exercise-trained mice depends on IL-15 in circulation, demonstrating that IL-15 is an important anti-aging exercise signal.

Results

Epidermal aging is associated with mitochondrial dysfunction

Although the structural deterioration and slow healing evident in aged skin have been known for some time, we are only just beginning to understand the mechanisms that drive chronological skin aging. Wound closure is the primary end point used to assess healing therapy efficacy (25), so identifying age-related factors that regulate keratinocyte maintenance or re-epithelialization is a logical starting point to understand the basis of healing defects. Previous research implicates senescent cells (9, 10, 26, 27), inflammation (11), and dendritic T-cells (9, 10) in skin aging and the resulting impairment in re-epithelialization. To gain additional insight into the underlying mechanisms of aging within the epidermis, we re-analyzed a publicly available gene expression dataset comparing FACS-sorted young and old murine epidermal stem cells (ESCs, $CD49f^{high}/CD34^{-}$) collected from uninjured dorsal skin that originally examined age-related changes in circadian rhythms (GSE84511) (28). We analyzed differentially expressed genes in young *versus* old ESCs irrespective of the time of day ($n = 24$ per age group), giving us substantial power to detect aging effects, and then employed two established differential gene expression analysis tools, GAGE (generally applicable gene set enrichment for pathway analysis) (29) and GSEA (gene set enrichment analysis) (30). GAGE evaluates significantly differentially expressed genes without an arbitrary fold-change cut-off to identify sets of coordinately perturbed genes (up and/or down) and their related pathways, increasing the sensitivity and reproducibility of pathway analysis (29). Our GAGE analysis identified several significantly altered pathways previously associated with ESC aging such as JAK/STAT signaling and senescence as shown by simultaneous aging associated elevations in canonical STAT signaling with prosurvival (Akt), cell cycle arrest (Cyclin D1), and anti-apoptotic signaling (Bcl-Xl) (Fig. 1*A*, and Fig. S1, *A* and *B*). Additionally, GAGE highlighted pathways that have never been connected to ESC aging, including the cellular energy sensor AMP-activated protein kinase (AMPK) and metabolic peroxisome proliferator-activated receptor (PPAR) signaling (Fig. 1*A*). Pathview is a graphical display package that overlays gene expression metrics on Kyoto Encyclopedia of Genes and Genome (KEGG) pathway diagrams. Detailed networks of the JAK/STAT pathway and AMPK signaling alterations using Pathview show comprehensive downstream pathway dysregulation (up and down) in response to aging (Fig. S1, *A* and *B*). Subsequently, GSEA analysis was used to identify cellular functions consistently up-regulated or consistently down-regulated in response to aging. We found that metabolic pathways related to glucose and carbohydrate metabolism were up-regulated and that mitochondrial synthesis and ATP production were down-regulated in aged ESCs (Fig. 1*B*), suggesting a shift away from oxidative phosphorylation-derived cellular energy. A selection of differentially expressed genes from the identified pathways highlights these changes (Fig. 1*C*). Age-induced mitochondrial deterioration is well-described in other stem cells such as muscle and neural progenitors (31), but these data provide the first evidence that the epidermal stem cell compartment experiences broad metabolic dysfunction during aging. Together, these data suggest that mitochondrial defects are mirrored across multiple cell types in aging skin and may drive its aging process.

Administration of IL-15 to sedentary mice rescues defective would closure

We have previously shown that IL-15 reverses skin aging in intact skin, but the impact of low dose rmIL-15 treatment on skin healing has not been established. Interestingly, IL-15 receptor α subunit expression (IL-15Rα) was identified through our pathway

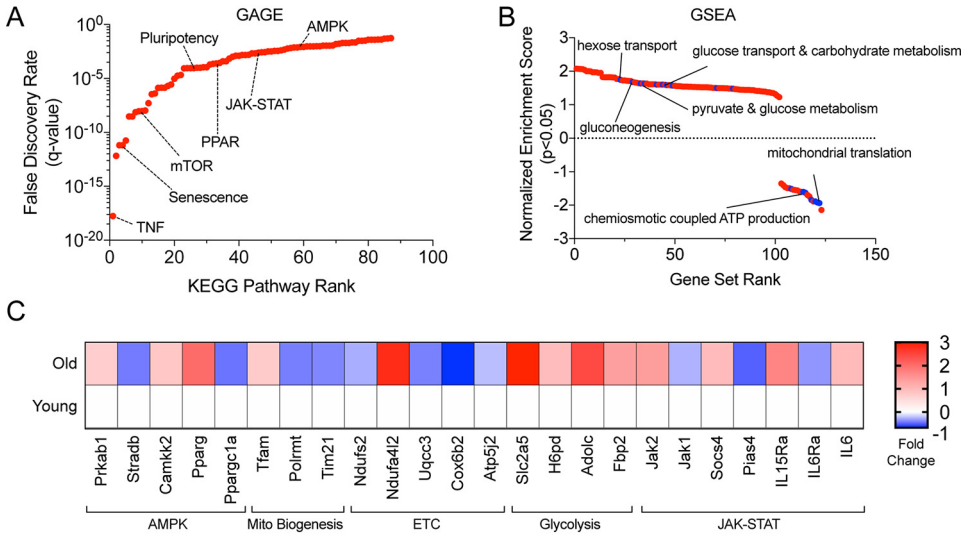

Figure 1. Metabolic dysfunction is a hallmark of aged murine epidermis. *A,* bidirectional KEGG (Kyoto Encyclopedia of Genes and Genomes) pathway perturbation analysis using GAGE depicting significant defined biological pathways (KEGG Pathways) with genes significantly up and/or down with age. *B,* unidirectional GSEA showing sets of genes either up or down with age associated with specific gene ontology terms. Gene ontologies are ordered by their normalized enrichment score that signifies how uniform the gene expression change is across all member genes of a set (Gene Set Rank). *C,* candidate differentially expressed genes in young *versus* old mouse epidermal stem cells. All analysis in *A–C* was generated using raw data from GSE84511. Significance was determined by a Benjamini-Hochberg False Discovery Rate adjusted $p < 0.05$.

analysis to be increased in old *versus* young epidermal stem cells (Fig. 1*C*), which is analogous to greater IL-15Rα expression levels found in nonhealing *versus* healing wounds in humans (24). Moreover, Keyes *et al.* (9) identified IL-15 as one of a handful of down-regulated genes in old *versus* young mouse epidermal keratinocytes isolated from the leading wound edge and circulating IL-15 levels are reduced in old mice (23). In combination this suggested that IL-15 treatment may improve wound healing in aged skin. To assess this, we used our previously described regimen of IL-15 therapy in which aged mice were pre-treated for 33 days with daily intravenous rmIL-15 (old rmIL-15, 25 ng/kg) or PBS vehicle injections (old controls) as well as a young, PBS-injected control group (20). After this pre-treatment phase, excisional wound surgery was performed and the closure of wounds was tracked over 9 days, which is the approximate time to full wound closure in young mice. Splinted, full-thickness wounds were utilized to prevent confounding wound contraction prevalent in murine wounds and to promote greater re-epithelialization akin to human wound healing as described by others (32). Due to the long wound healing period after pre-treatment and the rapid turnover rate of the murine epidermis (33), we continued daily injection treatments of rmIL-15 or vehicle control until 5 days post-surgery (Fig. 2*A*). The young control group was largely fully healed after 9 days (>95% original wound area healed), whereas old control mice had significantly less advanced wound closure at 9 days post-wounding (Fig. 2, *B–D*). Remarkably, we found that rmIL-15 treatment in old mice resulted in significantly smaller wounds at 9 days post-wounding compared with old controls and their degree of healing was indistinguishable from young control mice (Fig. 2, *B–D*). We also analyzed the rate of wound closure over time and this showed a significantly decreased wound closure rate in the old PBS group relative to young PBS, but a restoration of healing rate in rmIL-15–treated old mice (Fig. 2*E*). Additionally, when we extrapolated these healing rates to time until full wound closure, we found that old control mice were projected to heal ~2 days slower than both young control and old rmIL-15–treated groups (Fig. 2*F*).

It has been recently shown that a transiently thickened region of Keratin 14-positive epidermal progenitors forms inward from the original wound margin, termed the proliferative hub (34). This thickened hub sustains the extending epithelium as the wound closes but resolves and thins when re-epithelialization is completed. This phenomenon has not yet been investigated in aged mouse skin, so we sought to use it to better understand the impact of our therapy on the extent of re-epithelialization. Thus, we stained day 9 post-wounding skin cross-sections for Keratin 14 and 5-ethynyl-2′-deoxyuridine (EdU) incorporation and assessed the average thickness of the Keratin 14 layer 300 μm toward the center of the wound from the original wound margin guided in part by EdU staining. We found that old control mice had a hyper-thickened proliferative hub at day 9 post-wounding compared with young controls, suggesting a less advanced stage of re-epithelialization, however, the old rmIL-15–treated group had a reduced proliferative hub thickness compared with old controls and this thickness was indistinguishable from young mice (Fig. 2, *G* and *H*). Thus, short-term IL-15 therapy is able to restore a youthful rate of skin healing in aged mice.

Recombinant IL-15 therapy rescues age-associated changes in STAT3 and cellular senescence in vivo

Because STAT3 signaling is implicated in keratinocyte aging (9), we sought to clarify how it was impacted by aging and IL-15 therapy *in vivo*. Using the intact skin excised during wound surgery, we found that staining for nuclear STAT3 phosphorylated at tyrosine 705 (pSTAT3^{Y705}) was higher in interfollicular epidermal cells and dermal fibroblasts (vimentin$^+$ dermal cells) of old control mice compared with young controls, however, rmIL-15 treatment largely abrogated this elevation in both cell

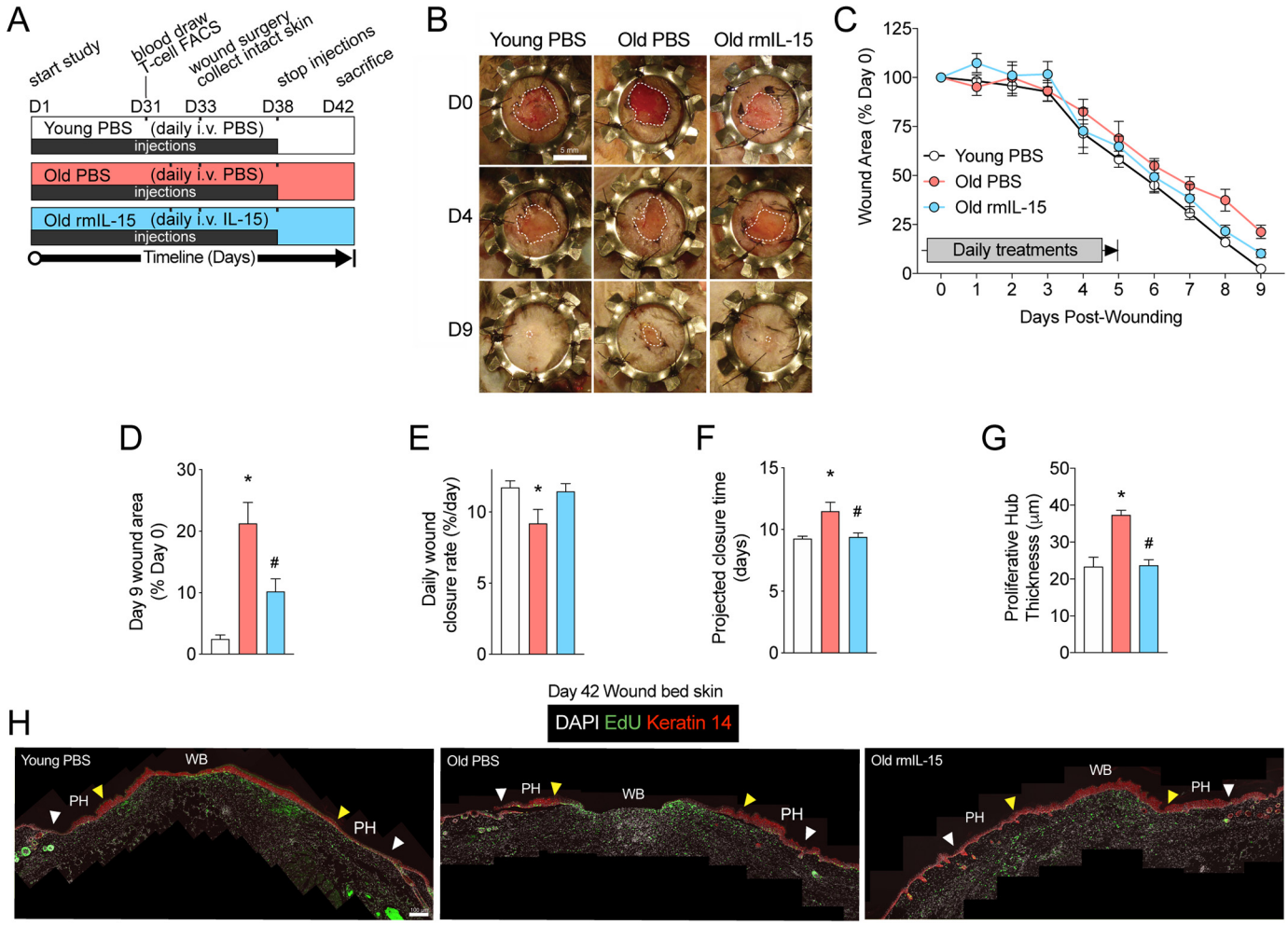

Figure 2. Exogenous IL-15 therapy rescues wound healing in aged, sedentary mice. *A,* experimental design of intravenous pre-treatments and wound surgery with key experimental days denoted on a timeline. *B,* representative photographs of wound healing progress in young control (*Young PBS*), old control (*Old PBS*) and old IL-15 (*Old rmIL-15*)–treated mice on the indicated days post-wounding. Wound margins are delineated by the *dotted white line*. *Scale bar* = 5 mm. *C,* quantification of wound areas from *B*. *D,* final wound closure at time of sacrifice on day 9 expressed as a proportion of the original wound area. *E,* wound closure rate per day determined by average slope of best fit lines. *F,* projected time for full wound closure based on wound closure rate calculated in *E*. $n = 4–8$ mice per group for *A–E* data. *G,* quantification of Keratin 14-stained proliferative hub thickness in young PBS, old PBS, and old rmIL-15–treated mice. $n = 3–5$ mice per group. *H,* stitched panoramic immunofluorescence images of Keratin 14-stained stem cells and EdU labeling in day 9 post-wounded skin showing the wound bed (*WB*) and proliferative hub (*PH*) region of each side. *White arrow* (original wound edge) to and the *yellow arrow* (300 μm inwards) indicates the proliferative hub region. *Scale bar* = 100 μm. Data are mean ± S.E. *, significantly different ($p < 0.05$) relative to Young PBS mice. #, significantly different ($p < 0.05$) relative to Old PBS mice.

types (Fig. 3, *A* and *B*). Conversely, STAT3 phosphorylation at its Ser-727 site (pSTAT3^{S727}) was reduced in old *versus* young control mice yet restored in old rmIL-15–treated mice (Fig. 3, *A* and *C*). Thus, the two STAT3 regulatory sites are altered in opposite directions by both aging and rmIL-15 treatment within the epidermis and dermal fibroblasts. Because we have previously shown our rmIL-15 regimen increases mitochondrial activity in whole mouse skin and within cultured human fibroblasts (20), we sought to assess whether these changes occurred in isolated epidermis. Thus, we measured complex IV activity in whole epidermal protein lysates from each group. We found that complex IV activity tended to be reduced in young *versus* old control mice ($p = 0.097$, Fig. S2*A*). Additionally, old mice treated with rmIL-15 had significantly greater complex IV activity than old control mice (Fig. S2*A*). These data show that rmIL-15 treatment augments epidermal mitochondrial function.

Cellular senescence has also been implicated as a driver of aging in numerous tissues (35) and biomarkers of senescence, such as the loss of nuclear proteins HMGB1 or Lamin B1 occur more frequently in aged skin (36–38). Thus, an increased burden of growth-arrested cells is a logical explanation for at least some of the age-associated delays in cell growth during wound healing. Given the improved cellular re-growth after injury found in old rmIL-15–treated mice, we reasoned that this treatment would be associated with a lower burden of cellular senescence. To assess senescence, we quantified the presence or absence of nuclear HMGB1 and nuclear Lamin B1 levels via immunofluorescence in intact skin samples collected during wound surgery. We found that nuclear HMGB1 staining was reduced in epidermal cells and dermal fibroblasts of old control mice relative to young control, but that this loss was not observed in the old rmIL-15–treated mice (Fig. S2, *B* and *C*). However, the aging-associated loss of nuclear Lamin B1 ob-

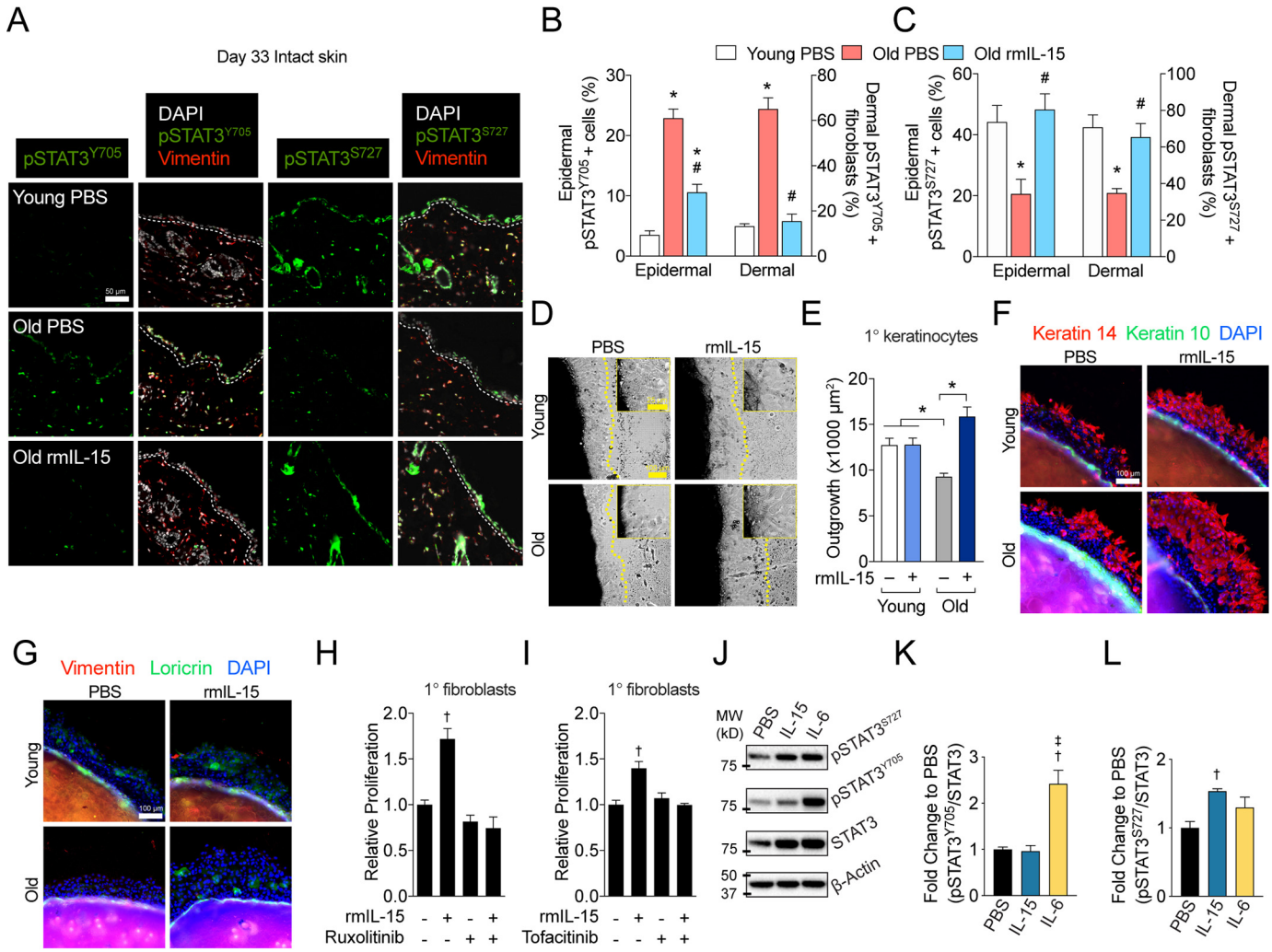

Figure 3. Exogenous IL-15 therapy rescues STAT3 phospho-signaling and cell growth in aged, sedentary mice. *A*, representative images of pSTAT3^{Y705} and pSTAT3^{S727} immunofluorescence staining in intact skin collected during wound surgery (day 33 of treatment). The epidermal basement membrane is indicated by the *white dashed line*. *Scale bar* = 50 μm. *B* and *C*, quantification of staining shown in *A* in epidermal cells and dermal fibroblasts. $n = 4–8$ mice per group. *D*, brightfield images and magnified insets of young and old skin explants after 48 h of treatment with or without 100 pg/ml of rmIL-15. *Scale bar* = 100 μm. *Inset scale bar* = 25 μm. *Dashed lines* indicate the borders of keratinocyte outgrowth and *E*, quantification of outgrowth area. $n = 3$ per treatment. *F*, representative images of Keratin 14 and Keratin 10, as well as, *G*, Loricrin and vimentin immunofluorescent staining from young (3 months) and old (25 months) skin explants after 48 h of growth. *Scale bar* = 100 μm. *H* and *I*, relative counts of primary dermal fibroblasts after 72 h of treatment of 100 pg/ml of rmIL-15 following 3 h of pre-treatment with either 0.4 μg/ml of ruxolitinib (*H*) or 0.4 μg/ml of tofacitinib (*I*). *J*, representative Western blots with molecular weight (*MW*) indicators and quantification of (*K*) STAT3 Tyr-705 and (*L*) Ser-727 phosphorylation in primary dermal fibroblasts treated with PBS, 100 pg/ml of rmIL-15, or 100 ng/ml of rmIL-6 for 30 min. $n = 5$ per treatment. Data are mean ± S.E. *, significantly different ($p < 0.05$) relative to Young PBS mice. #, significantly different ($p < 0.05$) relative to Old PBS mice †, significantly different ($p < 0.05$) relative to PBS control. ‡,Significantly different ($p < 0.05$) relative to rmIL-15.

served in old control mice compared with young controls was only partially rescued by rmIL-15 treatment in the epidermis and was not impacted by rmIL-15 therapy in dermal fibroblasts (Fig. S2, *B* and *D*). The difference in response between senescence biomarkers is likely due to HMGB1 being more related to transient growth arrest (p53-related), whereas Lamin B1 is more reflective of terminal growth arrest (Rb/p16^{ink4a}). Taken together, IL-15 therapy reduces the proportion of senescent cells in aged skin.

IL-15's most well-established physiologic function is in innate immunity where it activates and expands T-cells and NK cells and this function has been leveraged as an immunotherapy to reduce the growth of some types of cancers (21). However, IL-15's effects on T-cell proliferation and its anti-tumor activity typically require at least 3 orders of magnitude higher dosing than the dose we utilized in our experiments (39). Nevertheless, because T-cells play a prominent role in wound healing (9), we wanted to assess the impact of our recombinant IL-15 treatment on this immune population. First, we assessed spleen weights across all of our treatment groups to ascertain any broad changes in immune system activation. Old mice had greater spleen weights (as a percent of body mass) compared with young mice, but this was similar between old control and old rmIL-15–treated mice (Fig. S2*E*). We then assessed T-cells in the epidermis by staining for the T-cell marker CD3 in day 33 intact skin collected during wound surgery. However, we found no differences between our treatment groups in the proportion of CD3$^+$ cells within the epidermis (Fig. S2*F*). Finally, we quantified circulating, peripheral blood cytotoxic T cells (CD3$^+$/CD8$^+$) by flow cytometry in our experimental cohort after 31 days of pre-treatment and just prior to wound surgery. Similar to epidermal T-cells, we found no changes in the abundance

of circulating cytotoxic T-cells across our treatment groups (Fig. S2G). Thus, our dose of IL-15 does not appear to expand circulating or resident epidermal T-cells or overtly activate the immune system in aged mice.

To gain further insight into how IL-15 was working, we next sought to examine whether this benefit was specific to aged skin. We repeated our experiment of 33 daily injections of rmIL-15 or PBS vehicle prior to wound surgery in young mice. We presumed that the rate of re-epithelialization and healing was somewhat maximal in young skin. In agreement with this hypothesis, we found that rmIL-15 treatment in young mice did not impact day 9 wound closure or the rate of wound healing compared with young control mice (Fig. S3, *A–D*). However, there was a modest trend for a reduction in projected time until closure (<1 day, $p = 0.0502$, Fig. S3*E*). This suggests that young skin is able to "catch up" at later stages of healing, which somewhat negates the benefits of IL-15 therapy. Because IL-15 treatment impacted pSTAT3 signaling in aged skin, we again measured the proportion of skin cells with strong nuclear $pSTAT3^{Y705}$ and cellular $pSTAT3^{S727}$ in tissue cross-sections. We found that rmIL-15 treatment in young mice only produced significant changes in interfollicular epidermal cells, but not dermal fibroblasts, reducing nuclear $pSTAT3^{Y705}$-positive cells and increasing $pSTAT3^{S727}$-positive cells compared with young vehicle controls (Fig. S3, *F–I*). Thus, recombinant IL-15 treatment does not appreciably impact healing in young mice and modestly alters STAT3 signaling in the epidermis.

IL-15 directly increases the cell growth of mouse fibroblasts and keratinocytes

Our data clearly show that low-dose IL-15 improves the pathophysiology of aged skin and its healing, but it was still unclear whether this was a direct, cell autonomous effect. We have previously shown that post-exercise levels of recombinant human IL-15 (10 pg/ml) stimulate human dermal fibroblast proliferation (20), so we mirrored these conditions using post-exercise levels of IL-15 found in mice (100 pg/ml). To examine whether low-dose IL-15 acts directly on mouse keratinocytes, we employed an explant culture method that recapitulates age-related growth defects *in vitro* and exposed young and old skin explants to vehicle or 100 pg/ml of rmIL-15 immediately after plating. After 48 h of treatment, young mouse keratinocytes had a larger average area of outgrowth than old keratinocytes and rmIL-15 treatment was able to rescue growth defects in old explants to that of young mice (Fig. 3, *D* and *E*). To more specifically characterize the cell composition of rmIL-15–stimulated cellular growth, we stained outgrowth for the epidermal stem cell marker Keratin 14, keratinocyte differentiation markers Keratin 10 and Loricrin, and the fibroblast marker Vimentin. We observed that virtually all of the rmIL-15–stimulated outgrowth from aged skin explants after 48 h of culture was positive for Keratin 14, with occasional Loricrin-positive cells and no visible Keratin 10 or Vimentin staining (Fig. 3, *F* and *G*). This demonstrates that rmIL-15 treatment rescues growth defects in aged skin explants primarily by augmenting epidermal stem cell growth. Finally, because we observe many parallel effects on both keratinocytes and fibroblasts *in vivo*, we sought to test the effect of 100 pg/ml of IL-15 on mouse fibroblast growth. Primary mouse dermal fibroblasts showed a significant increase in proliferation when exposed to rmIL-15 for 72 h and this effect is blocked when the cells are treated with the JAK inhibitors ruxolitinib or tofacitinib prior to rmIL-15 (Fig. 3, *H* and *I*). Thus, low dose IL-15 acts cell autonomously on mouse epidermal stem cells and fibroblasts to stimulate cell growth in a JAK-dependent manner. In a separate experiment, we measured the acute response of $pSTAT3^{Y705}$ and $pSTAT3^{S727}$ relative to total STAT3 in fibroblasts exposed rmIL-15 via Western blotting. Because the cytokine IL-6 is well-known to signal via STAT3 Tyr-705 phosphorylation, we used this as a reference for comparison. IL-15 treatment only increased $pSTAT3^{S727}$, whereas IL-6 only induced $pSTAT3^{Y705}$ compared with untreated cells (Fig. 3, *J–L*). Therefore, unlike the classical STAT3 activator IL-6, low-dose IL-15 increases $pSTAT3^{S727}$ and not $pSTAT3^{Y705}$.

Exercise improves wound healing in aged mice via IL-15 signaling

Exercise is one of the only interventions that has been shown to improve wound healing in both aged mice (18) and humans (19), however, the underlying mechanism of this effect is not known. Because our rmIL-15 therapeutic regimen mimics physiologic elevations of post-exercise IL-15 in circulation, we sought to test whether this signaling was essential for the benefits of exercise on wound healing in aged skin. Thus, we subjected 2 groups of old mice to daily treadmill exercise for 33 days, with one group receiving IL-15 neutralizing antibody treatment (Old EX-nAb) and the other receiving control IgG antibody (Old EX) prior to each exercise session. Additionally, we included young and old sedentary control groups (Young SED, Old SED) that also received daily IgG control antibody injections. After 33 days of pre-treatment, we again performed splinted wound surgery and monitored healing over 9 days. To sustain our therapeutic window and to be congruent with the prior work showing that exercise improves wound healing in old mice (18), we continued the exercise and injection treatments for 5 days post-surgery (Fig. 4*A*). As might be expected, the continuation of exercise treatment after wounding surgery produced significantly more variability in day 1 to 5 of healing than in sedentary mice. Despite this, we found that aging resulted in impaired healing by day 9 compared with young sedentary controls, yet exercise treatment reversed this effect in old exercised mice *versus* old sedentary mice (Fig. 4, *B–D*). Remarkably, old exercised mice receiving IL-15 neutralizing antibody had similar day 9 wound closure as the sedentary old mice, demonstrating that IL-15 signaling is essential for the effects of exercise to speed wound closure in aged skin (Fig. 4, *B–D*). There was no effect on the rate of wound healing across the 4 groups (Fig. 4*E*). Analyzing the projected time until full wound closure revealed a significant 1.5 day difference between young, sedentary control and old sedentary mice groups, but projected healing times for old exercised and old exercised with neutralizing antibody groups were not significantly different compared with the young group (Fig. 4*F*). We then measured the Keratin-14–positive epidermal proliferative hub using day 9 post-wounding skin tissue cross-sections. We again found

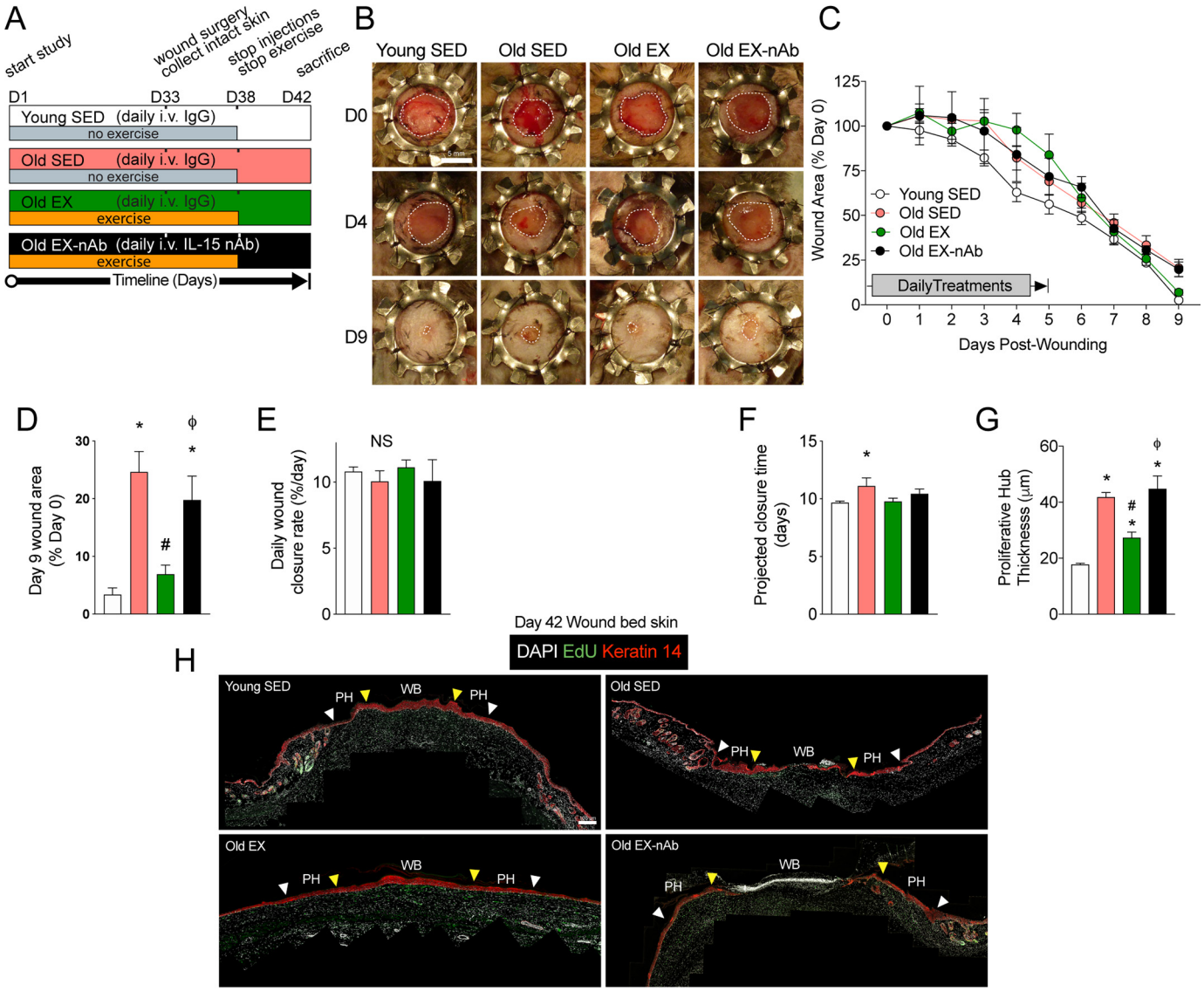

Figure 4. Exercise-induced improvements in wound healing depend on IL-15 signaling in aged mice. *A,* experimental design of intravenous pre-treatments, the exercise regimen, and wound surgery with key experimental days denoted on a timeline. *B,* representative images of wound healing progress in young sedentary (*Young SED*), old sedentary (*Old SED*), old exercised (*Old EX*), and old exercised mice receiving IL-15 neutralizing antibody (*Old EX-nAb*) on the indicated days post-wounding. Wound margins are delineated by the *dotted white line*. *Scale bar* = 5 mm. *C,* quantification of wound areas from *B*. *D,* final wound closure at time of sacrifice on day 9 expressed as a proportion of the original wound area. *E,* wound closure rate per day determined by average slope of best fit lines. *F,* projected time for full wound closure based on wound closure rate calculated in *E*. $n = 4–8$ mice per group in *A–E*. *G,* quantification of the proliferative hub thickness in each treatment group. $n = 3–5$ mice per group. *H,* stitched panoramic immunofluorescence images of Keratin 14-stained stem cells and EdU labeling in day 9 post-wounded skin showing the wound bed (*WB*) and proliferative hub (*PH*) region of each side. The space between the *white arrow* (original wound edge) and the *yellow arrow* (300 μm inwards) indicates the proliferative hub region. *Scale bar* = 100 μm. Data are mean ± S.E. *, significantly different ($p < 0.05$) relative to Young SED mice. #, significantly different ($p < 0.05$) relative to Old SED mice. φ, Significantly different ($p < 0.05$) relative to Old EX mice.

that old sedentary mice had a significantly thickened proliferative hub compared with young sedentary mice, however, this was reduced to the thickness of young mice in exercised old mice (Fig. 4, *G* and *H*). Importantly, old exercised mice that received IL-15 neutralizing antibody had greater proliferative hub thickness than old exercised and young sedentary mice (Fig. 4, *G* and *H*), further supporting the necessity of IL-15 for the beneficial effects of exercise on healing. These findings corroborate the work of others showing that exercise improves wound closure and re-epithelialization in old mice and we extend these results by showing that it depends on IL-15 in circulation.

Because rmIL-15 therapy in sedentary mice corrected age-induced changes in STAT3 signaling, we sought to examine this and additional aspects of mitochondrial and inflammatory signaling within our exercise experiment. Using intact skin excised during wound surgery, we again stained and quantified nuclear $pSTAT3^{Y705}$- and $pSTAT3^{S727}$-positive epidermal and dermal fibroblast cells. We found that old sedentary mice had more $pSTAT3^{Y705}$-positive cells than young mice but that this was abrogated in old exercised mice (Fig. 5, *A* and *B*). Additionally, old exercised mice receiving IL-15 neutralizing antibody had more $pSTAT3^{Y705}$-positive cells that young sedentary mice or old exercised mice (Fig. 5, *A* and *B*). Consistent with the

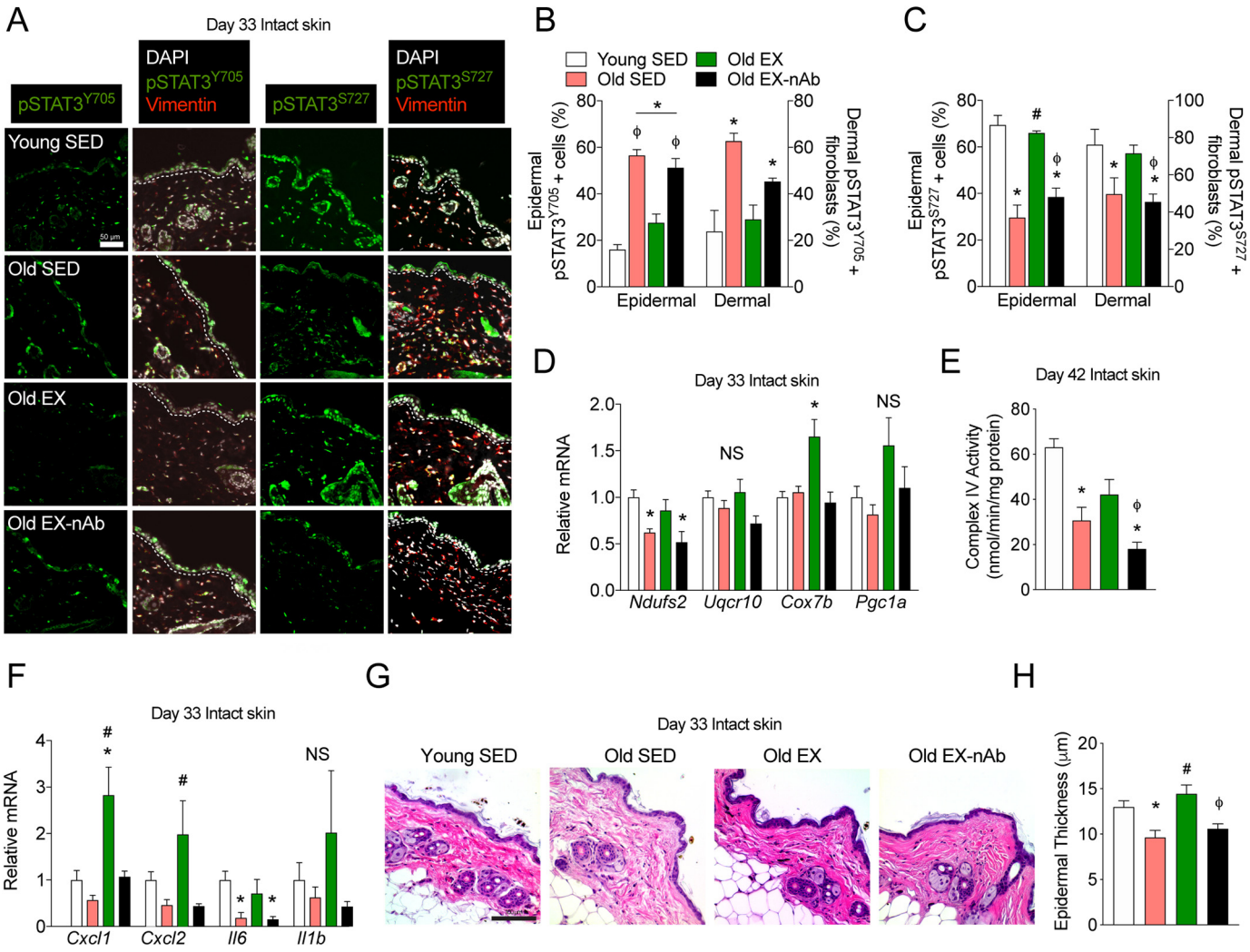

Figure 5. Neutralization of IL-15 in exercising mice prevents the rescue of STAT3 phospho-signaling, mitochondrial and inflammatory signaling, and epidermal structure. *A,* representative immunofluorescence images of pSTAT3^{Y705} and pSTAT3^{S727} staining in intact skin collected after 33 days of treatment in young sedentary (*Young SED*), old sedentary (*Old SED*), old exercised (*Old EX*), and old exercised mice receiving IL-15 neutralizing antibody (*Old EX-nAb*). The epidermal basement membrane is indicated by the *dashed white line*. *Scale bar* = 50 μm. n = 3–6 mice per group. *B* and *C,* quantification of epidermal cells and dermal fibroblasts for (*B*) pSTAT3^{Y705}-positive cells as well as (*C*) pSTAT3^{S727}-positive cells. n = 3–6 mice per group. *D,* mitochondrial epidermal mRNA expression in each treatment group relative to young control mice as measured by qPCR. n = 5–7 mice per group. *E,* mitochondrial cytochrome *c* oxidase activity measured on day 42 intact skin epidermal lysates. n = 3–5 mice per group. *F,* inflammation-associated epidermal mRNA expression in each treatment group relative to young control mice as measured by qPCR. n = 5–7 mice per group. *G,* brightfield microscopy images of hematoxylin and eosin-stained skin from each treatment group. *Scale bar* = 100 μm. *H,* quantification of epidermal thickness. n = 3–6 mice per group. Data are mean ± S.E. *, significantly different ($p < 0.05$ relative to young SED mice. #, significantly different ($p < 0.05$) relative to old SED mice. φ, significantly different ($p < 0.05$) relative to old EX mice. *NS*, nonsignificant ($p > 0.05$).

inverse relationship of pSTAT3^{S727}-positive cells to those with pSTAT3^{Y705}, we found fewer pSTAT3^{S727}-positive cells in old sedentary *versus* young sedentary mice (Fig. 5, *A* and *C*). In addition, old exercised mice had more pSTAT3^{S727}-positive cells than old sedentary animals, and this effect was lost in old exercised mice receiving IL-15 neutralizing antibody (Fig. 5, *A* and *C*). Thus, exercise reverses aging-induced changes in STAT3 signaling in skin and this depends upon circulating IL-15.

Given the dual role of the Tyr-705 and Ser-727 phosphorylation sites in regulating inflammatory and mitochondrial signaling, respectively, we sought to characterize downstream epidermal gene expression of these processes in response to aging and exercise. To capture *in vivo* gene expression changes in response to our treatment, we used whole epidermis separated from intact skin using dispase enzymatic digestion. Consistent with the down-regulation of mitochondrial signaling observed in aged ESCs (Fig. 1), we found lower mRNA expression of the mitochondrial complex I subunit *Ndufs2* in old sedentary mice compared with young sedentary mice (Fig. 5*D*). Interestingly, epidermal *Ndufs2* mRNA expression in old exercised mice was indistinguishable from young sedentary mice, but remained lower in old exercised mice receiving IL-15 neutralizing antibody (Fig. 5*D*). Additionally, whereas *Cox7B* mRNA was not altered in young sedentary *versus* old sedentary mice, it was significantly elevated in old exercised mice compared with young sedentary mice (Fig. 5*D*). However, old exercised mice treated with IL-15 neutralizing antibody exhibited no difference in *Cox7B* mRNA compared with young or old sedentary mice. There were no significant changes in the complex III sub-

unit *Uqcr10* or the mitochondrial regulator *Pgc1a* between treatment groups (Fig. 5*D*). To corroborate these mitochondrial changes, we again measured Complex IV activity in epidermal protein lysates. We found that old sedentary mice, but not old exercised mice, had significantly lower complex IV activity than young sedentary mice (Fig. 5*E*). Additionally, old exercised mice that received IL-15 neutralizing antibody had significantly reduced complex IV activity compared with young sedentary mice and old exercised mice (Fig. 5*E*).

When assessing epidermal inflammatory genes, we found that old exercised mice exhibited significantly higher *Cxcl1* mRNA than young control or old control mice, but old exercised mice receiving IL-15 neutralizing antibody had comparable expression to young and old control mice (Fig. 5*F*). Similarly, old exercised mice, but not exercised mice receiving IL-15 neutralizing antibody, had greater epidermal *Cxcl2* expression than old control mice (Fig. 5*F*). We also assessed the mRNA expression of the pro-inflammatory cytokine IL-6 (*Il6*), a classical activator of pSTAT3^{Y705} signaling, where we expected an age-induced elevation in *Il6* expression as seen in ESCs (Fig. 1*C*). Unexpectedly, we found that epidermal *Il6* was reduced in old *versus* young control mice, but was restored in old exercised mice to that of young control mice (Fig. 5*F*). Moreover, old exercising mice given neutralizing antibody had significantly lower *Il6* than young controls (Fig. 5*F*). Finally, we measured *Il1b* mRNA, but found no differences between treatment groups (Fig. 5*F*). Collectively, these data demonstrate that exercise depends upon circulating IL-15 to reverse aging-induced changes in epidermal mitochondrial and cytokine signaling. Finally, because we have shown that exercise and IL-15 therapy each independently reverse age-induced epidermal thinning, we sought to test if circulating IL-15 was essential for this effect of exercise in old mice. As we have previously observed, old control mice had reduced epidermal thickness *versus* young controls, but this was restored in old, exercised mice (Fig. 5, *G* and *H*). However, old exercising mice receiving IL-15 neutralizing antibody had significantly lower epidermal thickness that old exercised mice (Fig. 5, *G* and *H*), showing that exercise-induced IL-15 signaling is essential for the restoration of youthful epidermal structure.

Exercise-mediated changes in skin cell senescence partially depend upon circulating IL-15

Because recombinant IL-15 therapy was able to reverse the pattern of epidermal and dermal senescence in aged skin, we reasoned that exercise training in old mice would produce similar effects. Thus, we again assessed indicators of skin cell senescence (*i.e.* loss of nuclear HMGB1 or Lamin B1) in our exercise cohort. We found that the number of cells with nuclear HMGB1 in epidermal cells and dermal fibroblasts was again reduced in old *versus* young sedentary mice (Fig. S4, *A* and *B*). This loss of nuclear HMGB1 seen with aging was rescued in old exercised mice to that of young sedentary mice, however, the rescue was completely abrogated by IL-15 neutralizing antibody treatment (Fig. S4, *A* and *B*). Additionally, the proportion of epidermal cells and dermal fibroblasts with positive staining for nuclear Lamin B1 levels was reduced in old *versus* young sedentary mice but was restored to young levels in old exercised animals (Fig. S4, *A* and *C*). Old exercised mice receiving IL-15 neutralizing antibody had fewer dermal fibroblasts with nuclear Lamin B1 compared with old exercising mice, yet the proportion of epidermal cells with nuclear Lamin B1 was similar in old exercised mice treated with or without neutralizing antibody (Fig. S4, *A* and *C*). Additionally, there were no significant changes in the epidermal mRNA expression of the cell cycle regulators p21 or p16^{ink4a} in response to aging or exercise (Fig. S4*D*). Therefore some, but not all, of the benefits of exercise to mitigate skin growth arrest are derived from IL-15 signaling.

Discussion

The poor healing ability of aged skin is a major medical issue (2), but we lack therapies for this debilitating problem. Wound closure defects in the elderly are especially challenging to manage because this population frequently undergoes surgery, has a greater risk of open skin lesions (*i.e.* bedsores), and often suffers from disorders that impede tissue repair such as vascular disease or diabetes. The identification of new therapies to treat poorly healing wounds has stalled in recent decades and only 3 healing therapies have been approved for clinical use in the last 24 years (40). One reason for this lack of progress is that the underlying cellular defects responsible for aging are not well-understood and potential therapies must overcome impairments in signal transduction in aged cells (5). To begin addressing these problems we have used a highly powered bioinformatics approach to associate several known pathways of keratinocyte aging, such as JAK/STAT signaling and cellular senescence, to an area not previously connected to healing defects: bioenergetic dysfunction. We establish that daily pulses of IL-15 via injection or exercise, which boost mitochondrial abundance (20), restores youthful keratinocyte STAT3 signaling, reduces markers of growth arrest, and improves healing in aged skin. We observe that aging impedes wound healing by about 2 days, which is in line with the delay in healing observed in old *versus* young humans (41). Moreover, our finding that IL-15 can speed wound closure by ~2 days is similar to the improvement seen following becaplermin (platelet-derived growth factor) treatment in ischemic and hyperglycemic mouse models (42). However, in more severe clinical healing disorders, such as lower extremity ulcers, becaplermin treatment is able to reduce wound healing time by multiple weeks (43). Thus, IL-15 may have more substantial healing benefits if it is used to treat severe skin ulcers.

We opted to use intravenous tail vein injections to mirror the post-exercise secretions of IL-15 into the blood based around our prior work (20). We understand that a more practical delivery method is therapeutically desirable, however, drug delivery to the wound bed directly has its own confounding issues. First, healing wounds have a very proteolytic environment, so the bioavailability of rmIL-15 could be severely impacted and potentially in a different manner in young and old wounds. Second, most carrier formulations (*i.e.* ointments) make it difficult to visualize the leading edge of the wound for closure measurements. It is likely that a water-soluble small molecule would get around these issues, but this requires further investigation. Nevertheless, our data demonstrate that intravenous

IL-15 administration or exercise reverse fundamental aspects of skin aging and suggest that targeting these downstream molecular pathways can guide future efforts to improve poor skin healing.

Tissues directly involved in exercise such as skeletal muscle or the heart positively adapt over time to improve their physiological function. This adaptation occurs in response to a wide variety of cellular cues, including mechanical stress, calcium fluctuations, and other complex signals that would be difficult to recapitulate with drug injections (44). Thus, it is notable that a single factor such as IL-15 can enhance wound closure in aged skin and is the responsible exercise signaling factor for healing. We believe that IL-15 is effective for several reasons. First, healing is complex and treatments likely need to impact multiple facets of tissue remodeling and regrowth to be effective. We find that the actions of IL-15 are mirrored in keratinocytes and dermal fibroblasts *in vitro* and *in vivo*, suggesting direct, multipotent benefits of IL-15 treatment. Second, we find that IL-15 is able to reverse basic aspects of cellular aging, which likely permits enhanced tissue re-growth after injury. IL-15 restored epidermal mitochondrial (*Ndufs2*, *Cox7b*) and cytokine mRNA (*Il6*, *Cxcl1, Cxcl2*) as well as mitochondrial enzyme activity in aged epidermis. However, low dose IL-15 does not increase nuclear pSTAT3^{Y705}, suggesting a re-sensitization of keratinocyte recruitment or activation that became lost during aging. This idea fits well with prior research showing that circulating IL-15 is reduced in aged mice (23) and IL-15 mRNA expression is lower in old *versus* young keratinocytes at the leading edge of a healing wound (9). However, whether the loss of IL-15 signaling itself or other factors initially trigger skin aging and defects in tissue healing remains unknown.

Our understanding of how mitochondrial signaling and energy generation impact wound healing in the skin is limited, particularly in the context of intrinsic, chronological aging. However, there is some evidence for the involvement of mitochondrial deterioration in the other form of skin aging, UV radiation-induced photoaging. This type of aging is primarily due to exposure to UV-A and UV-B radiation in sunlight, which causes both nuclear and mitochondrial DNA damage and also increases the release of mitochondrial free radicals (8). Human photoaged skin exhibits a high incidence of large-scale mitochondrial DNA (mtDNA) deletions including two characteristic 3895- and 4977-bp common deletions that are significantly elevated compared with nonphotoaged skin from the same subject (45). These mtDNA deletions target portions of Complex I and IV, which impairs mitochondrial ATP generation (46).

The role of mitochondrial function in chronological aging-associated disease has been extensively investigated in other organs, however, its impact in the skin is relatively understudied. The most direct example of mitochondrial dysfunction in driving tissue aging is the progeroid aging phenotype of polymerase γ mutator mice (PolG mice) that have error-prone replication of their mtDNA (47). These animals systemically accumulate excessive mtDNA mutations, have reduced mitochondrial energy generation, and experience accelerated aging throughout the body including the skin. Notably, treatments that boost cellular metabolism such as endurance exercise (48) or the drug bezafibrate (49), rescues the epidermal, dermal, and subdermal adipose layer thinning of the skin observed in PolG mice. The striking reversal of progeroid aging in PolG mice by exercise training (48) was the initial catalyst for our previous investigation regarding exercise-induced circulating factors that impact skin aging (20). Based upon these initial observations in uninjured skin we now show that circulating IL-15 is part of a critical signaling circuit that restores aged skin repair through increased re-epithelialization and an enhancement in epidermal stem cell growth. Our findings add to the growing body of literature detailing how physical activity improves health and combats disease such as studies showing that exercise augments the post-injury repair of cardiac muscle (50) and peripheral nerves (51).

Unlike other stem cell populations, aging does not reduce the total number of epidermal stem cells, but does appear to stall their growth potential *in vitro* as well as their proliferation after wounding (9, 10). Although slow healing in aged skin has been associated with altered keratinocyte STAT3 signaling (9), there is little known about the role of cellular senescence. The delay in keratinocyte proliferation after wounding in healthy, aged mouse skin implies transient pausing of the cell cycle rather than extensive permanent growth arrest. Our data corroborate this idea and show that aging alters the alarmin and transient senescence marker HMGB1 but does not impact permanent senescence markers such as p16^{ink4a}. Additionally, we show that both HMGB1 and STAT3 dynamically respond to aging, exercise, and IL-15 treatment in the skin. This is not entirely unexpected as both factors activate pro-inflammatory processes after stress (38, 52, 53). Notably, a similar loss of HMGB1 has been associated with poor wound healing in diabetic skin and exogenous HMGB1 treatment restored diabetic healing defects (54), however, this prior study did not examine skin STAT3 signaling. Thus, changes in STAT3 may drive the loss of HMGB1 from the nucleus or vice versa to stall the cell cycle and delay re-epithelialization, but more work is needed regarding the interaction of these pathways in the context of wound re-epithelialization.

Although the biology of STAT3 has been extensively studied in disease, until now, all of our knowledge regarding STAT3 in aging skin has focused on its Tyr-705 phosphorylation site, which is well-established to increase in the aged epidermis (9, 55). However, no studies have previously characterized aging-induced changes to the STAT3 Ser-727 site. Classical pro-inflammatory cytokines such as IL-6 or granulocyte-macrophage colony-stimulating factor increase STAT3^{Y705} phosphorylation as well as induce senescence (56), and this class of cytokines is increased in the blood during aging as a consequence of low-grade inflammation (57). However, it has not been clear how one might physiologically reverse these cellular changes. Mechanistically, increasing pSTAT3^{S727} is one of the only known ways to promote dephosphorylation of pSTAT3^{Y705} via up-regulation of the phosphatase TC45 (58). At the same time pSTAT3^{S727} also directs the mitochondrial localization of STAT3 and the resulting enhancements in bioenergetic function (59). Because we show increased cellular pSTAT3^{S727} after IL-15 treatment and exercise, this seems the most likely explanation for the corresponding reduction in pSTAT3^{Y705}. Thus, there appears to be a counterbalancing role for

pSTAT3^{S727} in both cellular metabolism and cell growth during wound repair through moderation of pSTAT3^{Y705}-mediated signaling.

These studies expand our understanding of the health benefits of exercise in reducing the risk of age-related disease. Our findings suggest that other skin or epithelial disorders may be improved by regular exercise or conversely worsened by a sedentary lifestyle. Some indications of this connection have been established as vigorous physical activity adherence is associated with a lower risk of the inflammatory skin disorder psoriasis (60). Additionally, our findings have high translational potential as they are rooted in the physiologic exercise signaling observed in mice and humans and exercise is already known to improve healing in elderly subjects. Finally, higher doses of recombinant human IL-15 are already FDA approved for cancer immunotherapy, potentially reducing regulatory hurdles in applying a lower dose as a treatment for poorly healing wounds. Overall, these studies demonstrate that IL-15 therapy is a safe and efficacious means of reversing wound healing defects in aging skin.

Experimental procedures

Cell culture

Primary dermal fibroblasts were isolated by liberase (Sigma) enzymatic digestion of the underarm skin from adult female C57Bl/6 mice as described (61). Cells were cultured at 37 °C in Dulbecco's modified Eagle's medium (VWR) supplemented with 15% fetal bovine serum (Peak Serum), 1% glutamine (Gibco), 1% penicillin (Gibco), and 1% streptomycin (Gibco) under a 5% CO_2 atmosphere and experiments were performed on cells at passage 3–6. For proliferation, fibroblasts at approximate 70% confluence were first pre-treated with 0.4 μg/ml of ruxolitinib (Cayman), 0.4 μg/ml of tofacitinib (AdipoGen), or vehicle control (DMSO), and then 3 h later were treated with 100 pg/ml of rmIL-15 or vehicle (PBS). After 72 h, cells were counted using trypan blue dye exclusion on a hemocytometer. For STAT3 Western blotting, fibroblasts at ~70% confluence were treated with either vehicle control (PBS), 100 pg/ml of rmIL-15 (R&D Systems number 447-ML/CF), or 100 ng/ml of rmIL-6 (R&D Systems number 406-ML/CF) for 30 min. Cells were then collected in ice-cold RIPA lysis buffer (Boston BioProducts, 50 mM Tris-HCl, pH 7.4, 150 mM NaCl, 1% Nonidet P-40, 1% sodium deoxycholate, 0.1% SDS, 1 mM EDTA, 1 mM DTT, Pierce Complete Protease and Phosphatase inhibitor (Thermo Scientific)) and frozen in liquid nitrogen for later Western blotting.

Keratinocyte explant culture was performed by shaving and depilating telogen dorsal back skin from C57Bl/6 mice (3–5 months old for young and 23–24 months old for old) using clippers and NAIR before skin excision. The excised tissue was then incubated for 3 min in a solution of povidone/iodine, then twice in a solution of 70% ethanol for a total of 3 min, and finally rinsed in sterile PBS. The skin was then pinned epidermis side down and scraped with a beveled scalpel blade until all subdermal adipose had been removed and the dermis was abraded and translucent. A 4-mm biopsy punch was used to excise individual explants, which were plated dermis side down into a 24-well tissue culture plate (BioLite, Thermo) with a 1-h drying period to promote explant adhesion. Following the drying period, 400 μl of medium (Dulbecco's modified Eagle's medium supplemented with 15% fetal bovine serum, 1% glutamine, 1% penicillin, and 1% streptomycin) was added to submerge the explant. Explants were cultured at 37 °C with 5% CO_2 and cultured for 48 h after treatments before imaging cell outgrowth.

All fibroblast and keratinocyte explant experiments were performed in triplicate technical replicates to generate data for a single biological replicate (*i.e.* $n = 1$ for each unique mouse donor). Primary mouse fibroblast identity was determined by morphology. Primary mouse keratinocyte identity was confirmed by staining for Keratin 14, Keratin 10, or Loricrin as well as negative staining for Vimentin.

Tissue lysis and western blotting

Freshly dissected epidermis was separated from dermis using dispase (Roche) enzymatic digestion for ~1.5–2 h at 37 °C. Isolated epidermis was then homogenized in lysis buffer (50 mM HEPES, 150 mM NaCl, 100 mM NaF, 10 mM sodium pyrophosphate, 5 mM EDTA, 250 mM sucrose, 1 mM DTT, 1% Triton X-100, and Pierce Protease and Phosphatase Inhibitor solution (Thermo Scientific)). Primary dermal fibroblast and epidermal lysates were homogenized by freeze-thaw 3 times in liquid nitrogen followed by passage through a 27-gauge needle to ensure complete lysis. The protein concentration of epidermal lysates was assessed using a BCA kit (Pierce). For the fibroblast analysis of STAT3, 20 μg of protein per sample was prepared for SDS-PAGE by boiling in reducing 4× SDS-sample buffer (Boston BioProducts) for 5 min at 98 °C. Samples were loaded on a Mini-PROTEAN 4–15% TGX Stain-free Tris/Tricine precast gel (Bio-Rad) and run with Laemmli SDS-PAGE running buffer (Bio-Rad) for ~90 min at 100 V. Gels were semi-dry transferred onto polyvinylidene difluoride membranes using the Trans-Blot Turbo system (Bio-Rad) and all imaging was done with a ChemiDoc MP (Bio-Rad). Membranes were blocked and antibodies were diluted in Tris-buffered saline (TBS) with 0.1% Tween 20 and 5% BSA fraction V (Bio-Rad). Primary antibodies and their usage were as follows: β-actin (rabbit, Cell Signaling number 4967, 1:1000), total STAT3 (rabbit, Cell Signaling number 30835S, 1:1000), pSTAT3^{Y705} (rabbit, Cell Signaling number 9145, 1:1000), pSTAT3^{S727} (rabbit, Abcam number AB30647, 1:1000). Membranes were stripped and re-probed using Restore Western blotting Stripping Buffer (Thermo) between pSTAT3^{S727}, pSTAT3^{Y705}, and total STAT3. Secondary antibody used was anti-rabbit IgG-horseradish peroxidase (H+L) (goat, Bio-Rad, 1:1000) with Clarity Western ECL Substrate (Bio-Rad) solution. Band densitometry was measured in Image Lab (Bio-Rad) to quantify relative phosphorylation normalized to β-actin. Western blotting was performed in triplicate with three biologically unique primary fibroblast cultures.

Animals

All animals used for the chronological aging experiments were young, adult (3–5 months old) or old (23–24 months old) female C57BL/6 mice. Female mice were used because the thickness of the skin and the rate of wound healing differs

between male and female mice, and because female mice are less prone to fighting and barbering when group housed. Mice were randomly allocated to treatment groups prior to the interventions. During the study, mice were group housed except after wounding surgery when they were individually housed to minimize disturbance to the wound site. All mice were maintained in an AAALAC approved animal facility and all procedures were approved by the Northeastern University IACUC according to NIH standards.

In vivo treatments

Old exercising mice that received IL-15 neutralizing antibody or IgG control antibody were exercised daily on a 15-degree incline using a 6-lane rodent treadmill (Columbus Instruments) at 16 m/min pace after the initial 1 week ramp up from 10 m/min. Exercising mice underwent training for 33 days plus 5 days post-wound surgery but did not exercise on the day of surgery. Post-surgery the exercising mice ran at 8 m/min to minimize wound aggravation. rmIL-15 (R&D Systems number 447-ML/CF) was administered at 25 ng/kg of body weight by tail vein injection. IL-15 neutralizing antibody (R&D Systems number AF447) or normal goat IgG control antibody (R&D Systems number AB-108-C) was provided at 8,750 ng/kg of body weight, via tail vein injection daily prior to exercise. Compounds were administered between 2 and 4 h prior to treadmill exercise sessions, once daily for 38 consecutive days.

Wounding surgery

Prior to surgery, all mice were anesthetized with isoflurane, provided subcutaneous carprofen for pain relief (5 mg/kg) (TCL), and hair was shaved with clippers. The skin was then swabbed with povidone/iodine (APLICARE) and ethanol. Thereafter, two 6-mm diameter dorsal full-thickness wounds were excised using a dermal biopsy punch (Medline) and this sample was used for intact skin histology and mRNA analysis. Wounds were made in telogen skin in all experiments. Wounds were splinted using a 10-mm inner diameter stainless steel ring (Grainger) secured with 4–6 monofilament nylon 5-0 sutures (Oasis) and cyanoacrylate adhesive (Krazy glue) as described (32). A clean Tegaderm (3M Medical) wound dressing was loosely applied around the circumference of the mice over the wounds to cover the splinted wounds. Carprofen (5 mg/kg) was administered subcutaneously for the following 3 post-operative days. Starting on the day of surgery, wounds were photographed daily using a DMC-FZ70 camera (Panasonic) when the Tegaderm dressing was changed until 9 days post-surgery. Wound site photography lighting conditions and imaging parameters on the camera were kept identical between days. Proliferating cells were labeled using 100 mg/kg of BrdU (Sigma) that was administered intraperitoneally 24 h before wounding or 100 mg/kg of EdU (Cayman Chemical) that was administered intraperitoneally 24 h before sacrifice. Wound surgery occurred on day 33.

Histology and immunofluorescence

Tissues were fixed overnight in 10% neutral buffered formalin, stored in 70% ethanol at 4 °C, processed by automated tissue processor (Thermo HistoStar), and embedded in paraffin. A microtome (Leica) was used to cut 4-μm skin cross-sections, which were allowed to dry overnight before de-waxing and further processing. Heat-induced epitope retrieval was performed on de-waxed slides with either citrate or Tris-EDTA buffer prior to immunofluorescence staining. Skin cross-sections were blocked for 30 min at room temperature in 5% normal goat serum PBS, which was also the primary antibody diluent, unless the target was a phospho-protein in which case 5% normal goat serum TBS was used. Primary antibodies and their usage were as follows: $pSTAT3^{S727}$ (rabbit, Abcam number AB30647, 1:200), $pSTAT3^{Y705}$ (rabbit, 1:100, Cell Signaling number 9145), Keratin 14 (chicken, BioLegend number 906004, 1:500), Vimentin (chicken, ThermoFisher number PA1-10003, 1:2000), HMGB1 (rabbit, Abcam number AB79823, 1:250), Lamin B1 (rabbit, Abcam number AB16048, 1:1000), Keratin 10 (rabbit, BioLegend number 905404, 1:500), and Loricrin (rabbit, BioLegend number 905104, 1:500). Primary antibody incubations were carried out overnight at 4 °C except for Keratin 14, Keratin 10, Loricrin, and vimentin, which were 2 h at room temperature. Following either PBS or TBS wash, secondary detection antibodies conjugated with either Alexa Fluor-647 or Alexa Fluor-488 (Invitrogen) were diluted in either PBS or TBS at 1:200 and were applied for 30 min at room temperature. Mounting media with DAPI used was either ProLong Gold (Invitrogen) or Vectashield Vibrance (Vector Labs), which were used interchangeably and allowed to cure prior to imaging. EdU staining was done using the Click-iT EdU Alexa Fluor Imaging Kit (Invitrogen) according to the manufacturer's instructions following primary antibody staining but prior to secondary antibody incubations.

For immunofluorescence staining of skin explants, samples were grown on cover glass and surrounded by a sterile 0.5-mm press-to-seal silicone gasket (Invitrogen) to reduce staining volume. After 48 h of skin explant outgrowth, cells were fixed for 1 h at room temperature in 10% neutral buffered formalin followed by 10 min of cell permeabilization using 0.1% Triton X-100 in PBS. Cells were then blocked for 30 min in 5% normal goat serum in PBS followed by a 2-h room temperature incubation with primary antibody and 30-min room temperature incubation with secondary antibody as described above. Hard set mounting media with DAPI was applied and cured prior to imaging.

Hematoxylin and eosin staining was performed on 4-μm dewaxed sections using standard histology protocols using Gill's hematoxylin No.1 and eosin Y (Sigma). Colorimetric stained slides were mounted with Permount (Fisher). All brightfield imaging was done using an inverted EVOS XL (Life Technologies) microscope. All fluorescence imaging was performed on an Revolve R4 (Echo Labs) microscope equipped with Olympus UPlanFL ×10/0.30, and UPlanFL ×20/0.50 air objectives using DAPI, FITC, and Cy5 fluorescence channels.

Image analysis

All image processing and analysis was conducted using ImageJ FIJI (version 2.0.0-rc-69/1.52i, NIH), Photoshop CC 2019 (version 20.0.4, Adobe), and Illustrator CC 2019 (version 23.0.3, Adobe). Daily images of the wound site were used to quantify wound closure over time. Images were processed to

normalize camera distance and angle using the size of the metal splint as a standardization factor. Wound measurements were obtained by tracing the area of the visible wound margin on each day relative to the splint area. Wound closure over time was normalized as a percentage of the original day 0 wound. The rate of wound healing was analyzed by fitting wound closure on days 0–9 on a linear best fit line.

Immunofluorescence images first underwent thresholding over the entire image set of all samples from the experiment followed by manual counting of positive cells for at least 3 unique fields from each sample. All epidermal analyses only counted interfollicular epidermal cells and excluded hair follicles. Dermal fibroblasts were identified by vimentin staining. $pSTAT3^{Y705}$-positive cells were those that had overlap with their DAPI nuclear signal. $pSTAT3^{S727}$-positive cells were those that had a DAPI-associated cytoplasmic signal. HMGB1-positive cells were those that had overlapping signal with their nuclear DAPI signal. Lamin B1-positive cells were those that exhibited perinuclear signal relative to their DAPI signal. Vimentin-positive cells were those that had DAPI-associated periplasmic signal. Keratin 14-, Keratin 10-, and Loricrin-positive cells were those that had DAPI-associated cytoplasmic signal.

Average thickness of the epidermal proliferative hub was measured over 300-μm span from wound margin, guided by EdU staining along with reference to the subdermal adipose layer and serially sectioned H&E samples (34). Composite images for thickness analysis were tiled by manually registering images of $\times$10 fields with ~20% overlapping content using Photoshop (Adobe), and individual thickness measurements were taken using ImageJ FIJI (NIH). Epidermal thickness measurements were performed on H&E-stained nonwounded skin cross-sections as previously described (20) by measuring the orthogonal distance from the basement membrane to the end of the spinous layer several times over the interfollicular epidermis.

Keratinocyte outgrowth was imaged in a circular overlapping clockwise pattern from 12 o'clock 24 h after plating and areas of outgrowth were imaged at 48 h after plating. Outgrowth at 48 h post-explanting were measured, and the maximal area outgrowth field for each discrete outgrowth on each explant was recorded by tracing its outline and calculating the enclosed area using Illustrator (Adobe). The average of the 3 highest of these maximal outgrowth area fields was taken and used as representative growth from the explant. For each data point, this process was done 2 times on 2 different pieces of explant skin from the same mouse.

Gene expression

The epidermis was separated from dermis using dispase (Roche) enzymatic digestion for 2 h at 37 °C. After digestion, the epidermis was scraped using a scalpel blade and immediately frozen at −80 °C until later analysis. RNA was extracted by homogenizing separated epidermis in TRIzol (Invitrogen) reagent using a bead mill apparatus (MPBio 5G) followed by column purification (Zymo Direct-zol RNA mini prep), on column DNase treatment and subsequent elution. 300 ng of total RNA was then reversed transcribed to cDNA (ABI HC cDNA synthesis kit), diluted 1:30 in ultrapure water, and mRNA expression was assessed using qPCR with TaqMan or SYBR chemistry.

Flow cytometry

Whole blood was collected on day 31 of the rmIL-15 or exercise experiments from the submandibular vein. Blood was collected into K2-EDTA MiniCollectTubes (Greiner Bio-One) and red blood cells were lysed using PharmLyse (BD Biosciences). Lymphocytes were then pelleted and incubated with FITC-CD3 (BD Pharminigen number 553061) and APC-CD8 (BD Pharminigen number 561093) antibodies and analyzed in conjunction with unlabeled and compensation controls on a BD FACSAria instrument. Data analysis was done using FlowJo software for MacOSX.

Microarray analysis

Microarray data from GSE84511 (28) was obtained from GEO using the Bioconductor suite of tools in R (version 3.5.1) on MacOSX. Differential gene expression between young and old epidermal stem cells were obtained using the LIMMA package (version 3.36.2) to contrast all aged animal GSM entries against all young animal GSM entries using group-means parameterization, empirical Bayes statistics for differential expression, and Benjamini-Hochberg false discovery rate adjustment (62). Gene set enrichment analysis using the FGSEA package (version 1.6.0) (default pathways, $p.adj < 0.05$, 10,000 permutations) and bidirectional KEGG pathway analysis using the GAGE package (version 2.30.0) was performed on differentially expressed genes using mouse (mmu) gene sets for bioprocesses, molecular factors, and cellular compartments with wiring diagrams generated using the Pathview package (version 1.20.0) for GAGE (29, 30).

Cytochrome c oxidase activity

Cytochrome *c* oxidase activity was measured as the decrease of absorbance due to oxidation of cytochrome *c* in epidermal lysates as described previously (20). Briefly, sodium dithionite (Fisher, S310-100) was used to reduce cytochrome *c* (Sigma, C-2506) in assay buffer (50 mM potassium phosphate buffer with 1 mM EDTA, pH 7.4). Reduced cytochrome *c* was added to 20 μl of sample lysate/well in a 96-well plate and the absorbance at 550 nm was monitored over 90 s as a fitted linear slope ($R^2 > 0.95$). Samples were measured in duplicate and absolute enzyme activity was normalized to protein concentration.

$$\frac{(Slope_{average}/18.5)}{([Protein] \times Volume_{Sample})/1000} \quad \text{(Eq. 1)}$$

Statistical analysis

GraphPad Prism (version 7.0d) was used to calculate statistics. Data were log transformed or square root transformed prior to statistical analysis. Significance was set as $p < 0.05$. Comparisons of two groups were performed using a Student's *t* test. Comparisons of more than 2 treatment groups were analyzed using a one-way or two-way analysis of variance as appropriate for the number of treatment factors. If statistical significance was achieved via analysis of variance, specific differences

between groups were identified using Holm-Sidak or Tukey's post hoc analysis.

Author contributions—W. W. and J. D. C. conceptualization; W. W. and J. D. C. data curation; W. W., E. D. C., Y. K., A. K., and J. D. C. formal analysis; W. W., E. D. C., and J. D. C. supervision; W. W., E. D. C., Y. K., A. K., and J. D. C. investigation; W. W., E. D. C., and J. D. C. methodology; W. W. and J. D. C. writing-original draft; W. W., E. D. C., Y. K., A. K., and J. D. C. writing-review and editing; E. D. C., Y. K., A. K., and J. D. C. visualization; J. D. C. resources; J. D. C. funding acquisition; J. D. C. project administration.

Acknowledgments—We thank Y. Hsu for providing experimental feedback and advice and J. Monaghan for helpful comments on the results.

References

1. Guo, S., and Dipietro, L. A. (2010) Factors affecting wound healing. *J. Dent. Res.* **89,** 219–229 CrossRef Medline
2. Ashcroft, G. S., Mills, S. J., and Ashworth, J. J. (2002) Ageing and wound healing. *Biogerontology* **3,** 337–345 CrossRef Medline
3. Margolis, D. J., Bilker, W., Santanna, J., and Baumgarten, M. (2002) Venous leg ulcer: incidence and prevalence in the elderly. *J. Am. Acad. Dermatol.* **46,** 381–386 CrossRef Medline
4. Margolis, D. J., Bilker, W., Knauss, J., Baumgarten, M., and Strom, B. L. (2002) The incidence and prevalence of pressure ulcers among elderly patients in general medical practice. *Ann. Epidemiol* **12,** 321–325 CrossRef Medline
5. Gould, L., Abadir, P., Brem, H., Carter, M., Conner-Kerr, T., Davidson, J., DiPietro, L., Falanga, V., Fife, C., Gardner, S., Grice, E., Harmon, J., Hazzard, W. R., High, K. P., Houghton, P., Jacobson, N., *et al.* (2015) Chronic wound repair and healing in older adults: current status and future research. *Wound Repair Regen.* **23,** 1–13 CrossRef Medline
6. Sen, C. K., Gordillo, G. M., Roy, S., Kirsner, R., Lambert, L., Hunt, T. K., Gottrup, F., Gurtner, G. C., and Longaker, M. T. (2009) Human skin wounds: a major and snowballing threat to public health and the economy. *Wound Repair Regen.* **17,** 763–771 CrossRef Medline
7. López-Otín, C., Blasco, M. A., Partridge, L., Serrano, M., and Kroemer, G. (2013) The hallmarks of aging. *Cell* **153,** 1194–1217 CrossRef Medline
8. Birch-Machin, M. A., and Bowman, A. (2016) Oxidative stress and ageing. *Br. J. Dermatol.* **175,** 26–29 CrossRef Medline
9. Keyes, B. E., Liu, S., Asare, A., Naik, S., Levorse, J., Polak, L., Lu, C. P., Nikolova, M., Pasolli, H. A., and Fuchs, E. (2016) Impaired epidermal to dendritic T cell signaling slows wound repair in aged skin. *Cell* **167,** 1323–1338.e14 CrossRef Medline
10. Giangreco, A., Qin, M., Pintar, J. E., and Watt, F. M. (2008) Epidermal stem cells are retained *in vivo* throughout skin aging. *Aging Cell* **7,** 250–259 CrossRef Medline
11. Swift, M. E., Burns, A. L., Gray, K. L., and DiPietro, L. A. (2001) Age-related alterations in the inflammatory response to dermal injury. *J. Invest. Dermatol.* **117,** 1027–1035 CrossRef Medline
12. Swift, M. E., Kleinman, H. K., and DiPietro, L. A. (1999) Impaired wound repair and delayed angiogenesis in aged mice. *Lab. Invest.* **79,** 1479–1487 Medline
13. Sano, S., Itami, S., Takeda, K., Tarutani, M., Yamaguchi, Y., Miura, H., Yoshikawa, K., Akira, S., and Takeda, J. (1999) Keratinocyte-specific ablation of Stat3 exhibits impaired skin remodeling, but does not affect skin morphogenesis. *EMBO J.* **18,** 4657–4668 CrossRef Medline
14. Han, G., and Ceilley, R. (2017) Chronic wound healing: a review of current management and treatments. *Adv. Ther.* **34,** 599–610 CrossRef Medline
15. Beer, H. D., Longaker, M. T., and Werner, S. (1997) Reduced expression of PDGF and PDGF receptors during impaired wound healing. *J. Invest. Dermatol.* **109,** 132–138 CrossRef Medline
16. Chakravarty, E. F., Hubert, H. B., Lingala, V. B., and Fries, J. F. (2008) Reduced disability and mortality among aging runners: a 21-year longitudinal study. *Arch. Intern. Med.* **168,** 1638–1646 CrossRef Medline
17. Carli, F., and Zavorsky, G. S. (2005) Optimizing functional exercise capacity in the elderly surgical population. *Curr. Opin. Clin. Nutr. Metab. Care* **8,** 23–32 CrossRef Medline
18. Keylock, K. T., Vieira, V. J., Wallig, M. A., DiPietro, L. A., Schrementi, M., and Woods, J. A. (2008) Exercise accelerates cutaneous wound healing and decreases wound inflammation in aged mice. *Am. J. Physiol. Regul. Integr. Comp. Physiol.* **294,** R179–R184 CrossRef Medline
19. Emery, C. F., Kiecolt-Glaser, J. K., Glaser, R., Malarkey, W. B., and Frid, D. J. (2005) Exercise accelerates wound healing among healthy older adults: a preliminary investigation. *J. Gerontol. A Biol. Sci. Med. Sci.* **60,** 1432–1436 CrossRef Medline
20. Crane, J. D., MacNeil, L. G., Lally, J. S., Ford, R. J., Bujak, A. L., Brar, I. K., Kemp, B. E., Raha, S., Steinberg, G. R., and Tarnopolsky, M. A. (2015) Exercise-stimulated interleukin-15 is controlled by AMPK and regulates skin metabolism and aging. *Aging Cell* **14,** 625–634 CrossRef Medline
21. Steel, J. C., Waldmann, T. A., and Morris, J. C. (2012) Interleukin-15 biology and its therapeutic implications in cancer. *Trends Pharmacol. Sci.* **33,** 35–41 CrossRef Medline
22. Petersen, A. M., and Pedersen, B. K. (2005) The anti-inflammatory effect of exercise. *J. Appl. Physiol.* **98,** 1154–1162 CrossRef Medline
23. Quinn, L. S., Anderson, B. G., Strait-Bodey, L., and Wolden-Hanson, T. (2010) Serum and muscle interleukin-15 levels decrease in aging mice: correlation with declines in soluble interleukin-15 receptor α expression. *Exp. Gerontol.* **45,** 106–112 CrossRef Medline
24. Jones, A. M., Griffiths, J. L., Sanders, A. J., Owen, S., Ruge, F., Harding, K. G., and Jiang, W. G. (2016) The clinical significance and impact of interleukin 15 on keratinocyte cell growth and migration. *Int. J. Mol. Med.* **38,** 679–686 CrossRef Medline
25. Flanagan, M. (2003) Wound measurement: can it help us to monitor progression to healing? *J. Wound Care* **12,** 189–194 CrossRef Medline
26. Sorrentino, J. A., Sanoff, H. K., and Sharpless, N. E. (2014) Defining the toxicology of aging. *Trends Mol. Med.* **20,** 375–384 CrossRef Medline
27. Herbig, U., Ferreira, M., Condel, L., Carey, D., and Sedivy, J. M. (2006) Cellular senescence in aging primates. *Science* **311,** 1257 CrossRef Medline
28. Solanas, G., Peixoto, F. O., Perdiguero, E., Jardí, M., Ruiz-Bonilla, V., Datta, D., Symeonidi, A., Castellanos, A., Welz, P.-S., Caballero, J. M., Sassone-Corsi, P., Muñoz-Cánoves, P., and Benitah, S. A. (2017) Aged stem cells reprogram their daily rhythmic functions to adapt to stress. *Cell* **170,** 678–692.e20 CrossRef Medline
29. Luo, W., Friedman, M. S., Shedden, K., Hankenson, K. D., and Woolf, P. J. (2009) GAGE: generally applicable gene set enrichment for pathway analysis. *BMC Bioinformatics* **10,** 161 CrossRef Medline
30. Sergushichev, A. (2016) An algorithm for fast preranked gene set enrichment analysis using cumulative statistic calculation. *BioRxiv* 10.1101/0600/2 CrossRef
31. Zhang, H., Menzies, K. J., and Auwerx, J. (2018) The role of mitochondria in stem cell fate and aging. *Development* **145,** Dev143420 CrossRef Medline
32. Davidson, J. M., Yu, F., and Opalenik, S. R. (2013) Splinting strategies to overcome confounding wound contraction in experimental animal models. *Adv. Wound Care (New Rochelle)* **2,** 142–148 CrossRef
33. Koster, M. I. (2009) Making an epidermis. *Ann. N.Y. Acad. Sci.* **1170,** 7–10 CrossRef Medline
34. Aragona, M., Dekoninck, S., Rulands, S., Lenglez, S., Mascré, G., Simons, B. D., and Blanpain, C. (2017) Defining stem cell dynamics and migration during wound healing in mouse skin epidermis. *Nat. Commun.* **8,** 14684 CrossRef Medline
35. Childs, B. G., Durik, M., Baker, D. J., and van Deursen, J. M. (2015) Cellular senescence in aging and age-related disease: from mechanisms to therapy. *Nat. Med.* **21,** 1424–1435 CrossRef Medline
36. Freund, A., Laberge, R.-M., Demaria, M., and Campisi, J. (2012) Lamin B1 loss is a senescence-associated biomarker. *Mol. Biol. Cell* **23,** 2066–2075 CrossRef Medline

37. Wang, A. S., Ong, P. F., Chojnowski, A., Clavel, C., and Dreesen, O. (2017) Loss of lamin B1 is a biomarker to quantify cellular senescence in photo-aged skin. *Sci. Rep.* **7,** 15678 CrossRef Medline
38. Davalos, A. R., Kawahara, M., Malhotra, G. K., Schaum, N., Huang, J., Ved, U., Beausejour, C. M., Coppe, J.-P., Rodier, F., and Campisi, J. (2013) p53-dependent release of Alarmin HMGB1 is a central mediator of senescent phenotypes. *J. Cell Biol.* **201,** 613–629 CrossRef Medline
39. Zhang, M., Yao, Z., Dubois, S., Ju, W., Müller, J. R., and Waldmann, T. A. (2009) Interleukin-15 combined with an anti-CD40 antibody provides enhanced therapeutic efficacy for murine models of colon cancer. *Proc. Natl. Acad. Sci. U.S.A.* **106,** 7513–7518 CrossRef Medline
40. Eaglstein, W. H., Kirsner, R. S., and Robson, M. C. (2012) Food and Drug Administration (FDA) drug approval end points for chronic cutaneous ulcer studies. *Wound Repair Regen.* **20,** 793–796 CrossRef Medline
41. Holt, D. R., Kirk, S. J., Regan, M. C., Hurson, M., Lindblad, W. J., and Barbul, A. (1992) Effect of age on wound healing in healthy human beings. *Surgery* **112,** 293–297 Medline
42. Uhl, E., Rösken, F., Sirsjö, A., and Messmer, K. (2003) Influence of platelet-derived growth factor on microcirculation during normal and impaired wound healing. *Wound Repair Regen.* **11,** 361–367 CrossRef Medline
43. Smiell, J. M., Wieman, T. J., Steed, D. L., Perry, B. H., Sampson, A. R., and Schwab, B. H. (1999) Efficacy and safety of becaplermin (recombinant human platelet-derived growth factor-BB) in patients with nonhealing, lower extremity diabetic ulcers: a combined analysis of four randomized studies. *Wound Repair Regen.* **7,** 335–346 CrossRef Medline
44. Egan, B., and Zierath, J. R. (2013) Exercise metabolism and the molecular regulation of skeletal muscle adaptation. *Cell Metab.* **17,** 162–184 CrossRef Medline
45. Birch-Machin, M. A., and Swalwell, H. (2010) How mitochondria record the effects of UV exposure and oxidative stress using human skin as a model tissue. *Mutagenesis* **25,** 101–107 CrossRef Medline
46. Naidoo, K., Hanna, R., and Birch-Machin, M. A. (2018) What is the role of mitochondrial dysfunction in skin photoaging? *Exp. Dermatol.* **27,** 124–128 CrossRef Medline
47. Trifunovic, A., Wredenberg, A., Falkenberg, M., Spelbrink, J. N., Rovio, A. T., Bruder, C. E., Bohlooly, Y. M., Gidlöf, S., Oldfors, A., Wibom, R., Törnell, J., Jacobs, H. T., and Larsson, N.-G. (2004) Premature ageing in mice expressing defective mitochondrial DNA polymerase. *Nature* **429,** 417–423 CrossRef Medline
48. Safdar, A., Bourgeois, J. M., Ogborn, D. I., Little, J. P., Hettinga, B. P., Akhtar, M., Thompson, J. E., Melov, S., Mocellin, N. J., Kujoth, G. C., Prolla, T. A., and Tarnopolsky, M. A. (2011) Endurance exercise rescues progeroid aging and induces systemic mitochondrial rejuvenation in mtDNA mutator mice. *Proc. Natl. Acad. Sci. U.S.A.* **108,** 4135–4140 CrossRef Medline
49. Dillon, L. M., Hida, A., Garcia, S., Prolla, T. A., and Moraes, C. T. (2012) Long-term bezafibrate treatment improves skin and spleen phenotypes of the mtDNA mutator mouse. *PLoS ONE* **7,** e44335 CrossRef Medline
50. Vujic, A., Lerchenmüller, C., Wu, T.-D., Guillermier, C., Rabolli, C. P., Gonzalez, E., Senyo, S. E., Liu, X., Guerquin-Kern, J.-L., Steinhauser, M. L., Lee, R. T., and Rosenzweig, A. (2018) Exercise induces new cardiomyocyte generation in the adult mammalian heart. *Nat. Commun.* **9,** 1659 CrossRef Medline
51. Park, J.-S., and Höke, A. (2014) Treadmill exercise induced functional recovery after peripheral nerve repair is associated with increased levels of neurotrophic factors. *PLoS ONE* **9,** e90245 CrossRef Medline
52. Horiuchi, T., Sakata, N., Narumi, Y., Kimura, T., Hayashi, T., Nagano, K., Liu, K., Nishibori, M., Tsukita, S., Yamada, T., Katagiri, H., Shirakawa, R., and Horiuchi, H. (2017) Metformin directly binds the alarmin HMGB1 and inhibits its proinflammatory activity. *J. Biol. Chem.* **292,** 8436–8446 CrossRef Medline
53. Yu, H., Pardoll, D., and Jove, R. (2009) STATs in cancer inflammation and immunity: a leading role for STAT3. *Nat. Rev. Cancer* **9,** 798–809 CrossRef Medline
54. Straino, S., Di Carlo, A., Mangoni, A., De Mori, R., Guerra, L., Maurelli, R., Panacchia, L., Di Giacomo, F., Palumbo, R., Di Campli, C., Uccioli, L., Biglioli, P., Bianchi, M. E., Capogrossi, M. C., and Germani, A. (2008) High-mobility group box 1 protein in human and murine skin: involvement in wound healing. *J. Invest. Dermatol.* **128,** 1545–1553 CrossRef Medline
55. Doles, J., Storer, M., Cozzuto, L., Roma, G., and Keyes, W. M. (2012) Age-associated inflammation inhibits epidermal stem cell function. *Genes Dev.* **26,** 2144–2153 CrossRef Medline
56. Kojima, H., Inoue, T., Kunimoto, H., and Nakajima, K. (2013) IL-6-STAT3 signaling and premature senescence. *JAKSTAT* **2,** e25763 Medline
57. Franceschi, C., and Campisi, J. (2014) Chronic inflammation (inflammaging) and its potential contribution to age-associated diseases. *J. Gerontol. A Biol. Sci. Med. Sci.* **69,** S4–S9 CrossRef Medline
58. Wakahara, R., Kunimoto, H., Tanino, K., Kojima, H., Inoue, A., Shintaku, H., and Nakajima, K. (2012) Phospho-Ser727 of STAT3 regulates STAT3 activity by enhancing dephosphorylation of phospho-Tyr705 largely through TC45. *Genes Cells* **17,** 132–145 CrossRef Medline
59. Wegrzyn, J., Potla, R., Chwae, Y.-J., Sepuri, N. B. V., Zhang, Q., Koeck, T., Derecka, M., Szczepanek, K., Szelag, M., Gornicka, A., Moh, A., Moghaddas, S., Chen, Q., Bobbili, S., Cichy, J., *et al.* (2009) Function of mitochondrial Stat3 in cellular respiration. *Science* **323,** 793–797 CrossRef Medline
60. Frankel, H. C., Han, J., Li, T., and Qureshi, A. A. (2012) The association between physical activity and the risk of incident psoriasis. *Arch. Dermatol.* **148,** 918–924 Medline
61. Seluanov, A., Vaidya, A., and Gorbunova, V. (2010) Establishing primary adult fibroblast cultures from rodents. *J. Vis. Exp.* CrossRef Medline
62. Ritchie, M. E., Phipson, B., Wu, D., Hu, Y., Law, C. W., Shi, W., and Smyth, G. K. (2015) limma powers differential expression analyses for RNA-sequencing and microarray studies. *Nucleic Acids Res.* **43,** e47 CrossRef Medline